UCLA

Title

Fire-induced albedo change and surface radiative forcing in sub-Saharan Africa savanna ecosystems: Implications for the energy balance

Authors

Dintwe, Kebonye
Okin, Gregory S
Xue, Yongkang

RESEARCH ARTICLE

Key Points:
- Fires exerted far more radiative forcing than previously estimated
- The long-term effects of fire-induced albedo change were an order of magnitude greater than the short-term effects

Correspondence to:
K. Dintwe,
kdintwe@ucla.edu

Fire-induced albedo change and surface radiative forcing in sub-Saharan Africa savanna ecosystems: Implications for the energy balance

Kebonye Dintwe[1] iD, Gregory S. Okin[1] iD, and Yongkang Xue[1] iD

[1]Department of Geography, University of California, Los Angeles, California, USA

Abstract Surface albedo is a critical parameter that controls surface energy balance. In dryland ecosystems, fires play a significant role in decreasing surface albedo, resulting in positive radiative forcing. Here we investigate the long-term effect of fire on surface albedo. We devised a method to calculate short-, medium-, and long-term effect of fire-induced radiative forcing and their relative effects on energy balance. We used Moderate Resolution Imaging Spectroradiometer (MODIS) data in our analysis, covering different vegetation classes in sub-Saharan Africa (SSA). Our analysis indicated that mean short-term fire-induced albedo change in SSA was -0.022, -0.035, and -0.041 for savannas, shrubland, and grasslands, respectively. At regional scale, mean fire-induced albedo change in savannas was -0.018 and -0.024 for northern sub-Saharan of Africa and the southern hemisphere Africa, respectively. The short-term mean fire-induced radiative forcing in burned areas in sub-Saharan Africa (SSA) was 5.41 W m^{-2}, which contributed continental and global radiative forcings of 0.25 and 0.058 W m^{-2}, respectively. The impact of fire in surface albedo has long-lasting effects that varies with vegetation type. The long-term energetic effects of fire-induced albedo change and associated radiative forcing were, on average, more than 19 times greater across SSA than the short-term effects, suggesting that fires exerted far more radiative forcing than previously thought. Taking into account the actual duration of fire's effect on surface albedo, we conclude that the contribution of SSA fires, globally and throughout the year, is ~0.12 W m^{-2}. These findings provide crucial information on possible impact of fire on regional climate variability.

1. Introduction

For millions of years, fires have been an integral part of the Earth's biogeochemical processes and influenced land-atmosphere interactions [*Belcher et al.*, 2010; *Glasspool et al.*, 2004; *Pausas and Keeley*, 2009]. At local scale, fires play a critical role in influencing natural selection and plant evolution, a process that contributed to evolution and expansion of flammable ecosystems [*Bond and Keeley*, 2005]. Conversely, fire spread is facilitated by plant species that have evolved to withstand burning [*Liu et al.*, 2010]. Fires consume large quantities of biomass, release CO_2, and smoke (black carbon) into the atmosphere and deposit ash and charcoal onto the ground surface [*Jin and Roy*, 2005; *Smith et al.*, 2005]. The ash and charcoal deposition causes darkening of the ground surface, which reduces surface albedo especially at infrared wavelengths [*Roy et al.*, 2005; *Xue et al.*, 2004]. Albedo, defined as the ratio of the reflected solar radiation to the incoming solar radiation [*Ångström*, 1925], is the key component controlling surface energy balance over land, thereby driving local climate and ecosystem functions [*Dickinson*, 1983].

Fire-induced albedo change and associated radiative forcing have started to attract the attention of ecologists, climatologists, and policy makers [*López-Saldaña et al.*, 2014]. Recent studies show that in boreal forest, postfire albedo increases at weekly to yearly temporal scales and results in negative radiative forcing [*Flannigan et al.*, 2009; *Huang et al.*, 2014; *Jin et al.*, 2012; *Lyons et al.*, 2008; *Oris et al.*, 2013; *Randerson et al.*, 2006]. However, in dryland ecosystems such as savannas and grasslands, postfire albedo decreases and causes positive radiative forcing at weekly to yearly temporal scales [*Gatebe et al.*, 2014; *Jin and Roy*, 2005; *López-Saldaña et al.*, 2014]. In North American boreal forest the radiative forcing exerted by fire-induced albedo change ranges between -4.5 W m^{-2} and -1.3 W m^{-2} [*Jin et al.*, 2012; *Lyons et al.*, 2008], whereas in African and Australian savannas it has been reported to be between 0.1 W m^{-2} and 0.5 W m^{-2} [*Gatebe et al.*, 2014; *Jin and Roy*, 2005; *Myhre et al.*, 2005]. Despite the relatively small radiative forcing in savanna fires, their global contribution is important because savannas contribute more than 80% of global fires, have high fire

frequency, and are relatively evenly distributed between the northern and southern hemispheres [*Govaerts et al.*, 2002; *van der Werf et al.*, 2010].

General circulation models show that fire-prone ecosystems are warming rapidly as a result of climate change [*Intergovernmental Panel on Climate Change*, 2013; *Hartmann et al.*, 2013; *Knapp et al.*, 2008; *Randerson et al.*, 2006; *Shongwe et al.*, 2009]. Fires are likely to respond to climate change, because they are regulated by precipitation (fuel load) and temperature (fuel load dryness). The projected increase in air temperature and decrease in precipitation are likely to increase fire potential, frequency, intensity, and the length of the fire season particularly in the United States, South America, Africa, and Australia [*Liu et al.*, 2010; *Pechony and Shindell*, 2010]. The interaction and feedback between fire activity and climate change are of significant importance because fire-prone ecosystems are extensive, covering 40% of the Earth's land surface, and responsible for more than 85% of the global fires [*Bond et al.*, 2005; *Hao and Liu*, 1994; *Rundel et al.*, 2016; *Tansey et al.*, 2004].

In light of the projected increase in fire frequency it is imperative to comprehensively assess and quantify fire-induced albedo change and the associated surface shortwave radiative forcing (SSRF). In this study, we calculated SSRF taking into account the long-term fire-induced albedo change and duration of albedo recovery. To the best of our knowledge, all previous dryland studies have assessed "instantaneous" fire-induced albedo change to calculate SSRF [*Gatebe et al.*, 2014; *Jin and Roy*, 2005; *Lyons et al.*, 2008]. We argue that instantaneous change of fire-induced albedo and associated SSRF do not reflect the full impact of fire, thus underestimating the impact of fire on energy balance. Here we devised methods to calculate short-, medium-, and long-term albedo changes, and the associated SSRF in fire-prone ecosystems. Our time scale of analysis ranges from about 1 week to one full year.

We conducted our study in Africa, because it is the single largest continental source of burning biomass, with its fires responsible for about 50% of the total amount of area burned globally each year [*Cahoon et al.*, 1992; *Cooke et al.*, 1996; *D'Odorico et al.*, 2007; *Flannigan et al.*, 2009; *Hao and Liu*, 1994; *Riaño et al.*, 2007; *Ribeiro et al.*, 2008; *Roberts et al.*, 2009; *Scholes et al.*, 1996; *van der Werf et al.*, 2004, 2006]. Africa has the highest rates of fires with peak biomass combustion as high as 6×10^6 t of fuel per day in the southern hemisphere and 9×10^6 t per day in the northern hemisphere [*Roberts et al.*, 2009]. Further, *De Sales et al.* [2015] has shown that overall postfire albedo change results in a decrease in precipitation over sub-Saharan Africa, associated with the weakening of the West African monsoon's progression through the region. The landscape of Africa makes it an ideal place to study fire and its associated impact on climate change. The north-south and east-west geographical orientation of Africa's southern and northern hemispheres, respectively, provide an environment conducive to study the relationship between fire-induced albedo and environmental factors such as precipitation, vegetation structure, and land use type.

2. Materials and Methods

2.1. Study Area

The study was conducted in sub-Saharan Africa (SSA) savannas and grasslands (Figure 1). Africa has the largest area of savannas, covering more than 50% (1.8×10^7 km^2) of the continent's land surface [*Smit*, 2004]. The southern hemisphere of Africa (SHA) has the largest continuous stretch of savannas that cover an area of ~1.4×10^7 km^2 of land surface, whereas northern sub-Saharan Africa (NSSA), that is, Africa north of the equator and south of the Sahara, covers about 3×10^6 km^2 of land surface [*Archer et al.*, 2001; *Grace et al.*, 2006; *Scholes and Archer*, 1997; *Smit*, 2004].

2.2. Brief Description of Data Set Used

The Moderate Resolution Imaging Spectroradiometer (MODIS) burn product (MCD45A1 V005), Bidirectional Reflectance Distribution Function (BRDF)-Albedo Model Parameters (MCD43A1), BRDF-Albedo Quality (MDC43A2), Enhanced Vegetation Index (MOD13A1), and vegetation cover classes (MCD12Q1) were used for this analysis, covering the period of 2000–2015. They were acquired from NASA's Earth Observing System Data and Information System (http://reverb.echo.nasa.gov). All the MODIS products used in this analysis had a 500 m spatial resolution.

The MODIS burned area product, MCD45A1, provides the day(s) of the year when pixels burn. The product is generated using an algorithm that takes advantage of the spectral, temporal, and structural changes on the
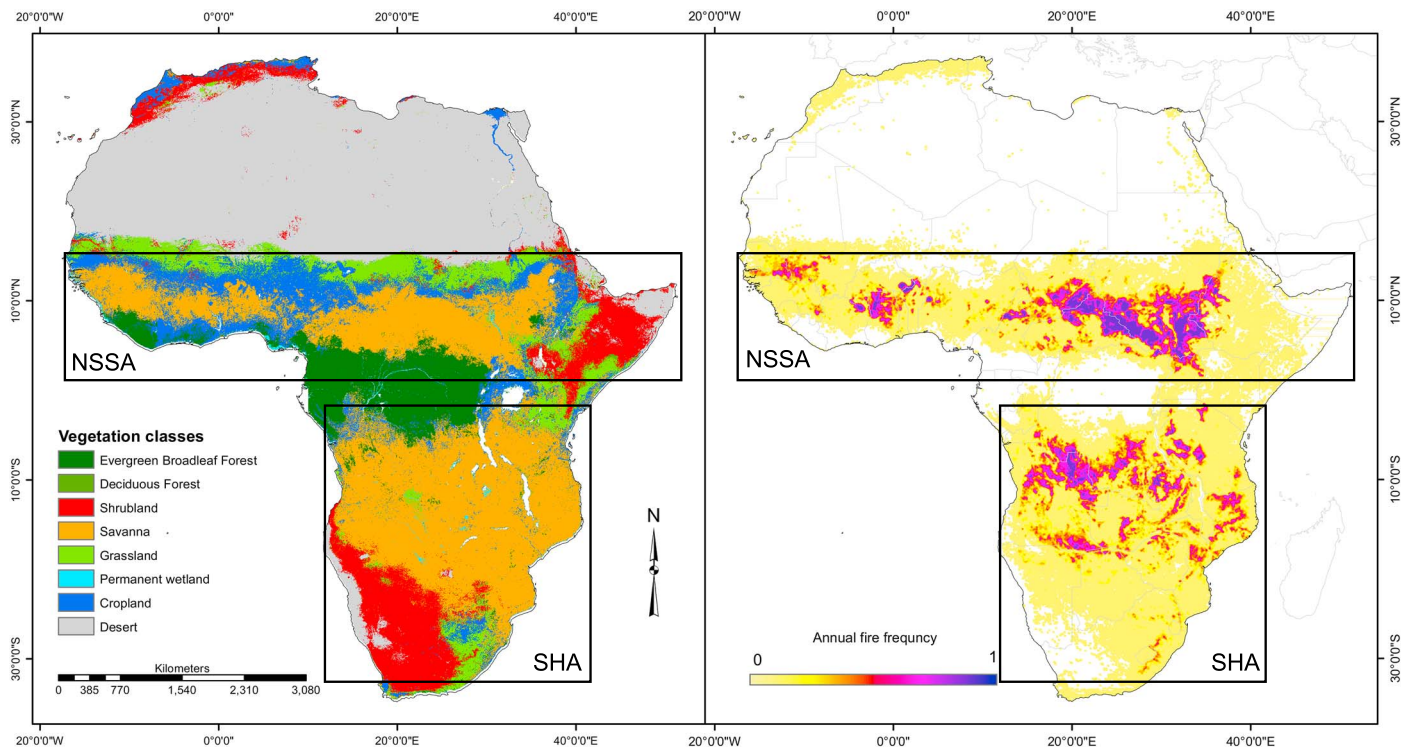
Figure 1. The map on the left shows the vegetation classes in Africa, following the International Geosphere-Biosphere Programme (IGBP) land cover classification. The map on the right shows the MODIS-derived fire frequency in Africa for the years 2000–2015. Regions used in this analysis are shown as boxes. NSSA is north sub-Saharan Africa, while SHA is the southern hemisphere Africa. The two regions together constitute sub-Saharan Africa (SSA).

land surface caused by deposits of charcoal and ash, removal of vegetation, and changes in vegetation structure [*Roy et al.*, 2008, 1999]. There are two standard MODIS products that provide direct information about area burned. The MODIS burned area product (MCD45) identifies fires through the detection of sudden changes in surface reflectance [*Roy et al.*, 2008]. The MODIS active fire product (MCD14ML) identifies fires through heat signatures identified in the thermal infrared [*Giglio et al.*, 2003]. In this study, the focus is on nonforest land cover classes (Table 1), which make up the vast majority of land in sub-Saharan Africa. *Roy et al.* [2008] have reported that the MODIS burned area product identifies burned areas at a rate greater than the active fire product for the nonforest classes examined here. This is because the burned area product is insensitive to the time of satellite overpass and is thus also less sensitive to the presence of obscuring clouds or smoke. Insensitivity to the time of satellite overpass is particularly important for fast-burning fires, like those that occur in the grassy savannas, grasslands, shrublands, and croplands that

Table 1. Annual Fire Regime in Africa Ecosystems, Over a 15 Year Period (2001–2015)

Region	IGBP Vegetation Class	Vegetation Class Area ($\times 10^6$ km^2)	(%) Area Total Land Surface	Burn Area km^2 yr^{-1} ($\times 10^3$)	Average Annual Ecosystem Burn (%)	Contribution to Regional Burn Area (%)	% Burn to Total Land Surface
North sub-Saharan Africa (NSSA)	Savanna	3.3	13.0	746.9	22.4	85.2	2.9
	Grassland	2.4	9.6	48.6	2.0	5.6	0.2
	Shrubland	2.1	8.4	5.8	0.3	0.7	0.0
	Cropland	16.3	63.5	74.7	0.5	8.6	0.3
South Hemisphere Africa (SHA)	Savanna	5.6	58.1	678.2	12.0	87.7	7.0
	Grassland	0.7	6.7	32.9	5.0	5.8	0.3
	Shrubland	1.5	15.3	14.6	1.0	2.8	0.2
	Cropland	0.8	8.4	18.4	2.3	3.4	0.2
Sub-Saharan Africa (SSA)	Savanna	9.0	25.3	1425.0	15.9	87.7	9.9
	Grassland	3.1	8.8	81.5	2.6	5.0	0.5
	Shrubland	3.6	10.3	20.3	0.6	1.3	0.2
	Cropland	17.2	48.4	93.1	0.5	5.9	0.5

dominate sub-Saharan Africa; due to their speed, fast-burning fires have a lower probability of detection from a satellite passing overhead.

The MODIS albedo products are generated through an algorithm that applies semiempirical kernel-driven bidirectional reflectance (BRDF) model using multidate, multispectral, and atmospherically corrected surface reflectance data to generate 16 day combined product, with 8 day overlap [*Schaaf et al.*, 2002]. The Enhanced Vegetation Index (EVI; MOD13A1) is a 16 day product that improved sensitivity, compared to NDVI, over high- and low-biomass regions through a decoupling of the canopy and soil backgrounds and atmospheric effects [*Huete*, 2012]. For vegetation cover classes, we used *International Geosphere-Biosphere Program* (*IGBP*) vegetation classes retrieved from the MCD12Q1 yearly MODIS land cover product [*Friedl et al.*, 2010].

Monthly downward shortwave radiation flux (DSWRF) and precipitation data at 0.25° and 0.5° spatial resolution, respectively, from 2000 to 2014 were used in this analysis [*Liu et al.*, 2012; *Rodell et al.*, 2004]. DSWRF data were obtained from Global Land Data Assimilation System, NOAH model (https://mirador.gsfc.nasa.gov).

2.3. Image Processing Albedo, EVI, and Burn Products

Monthly burn products were composited into yearly results. In the case where a pixel had more than one fire occurrence in a year, the last burn date was retained. The cases in which a pixel had more than one fire in a single year contributed about 0.05% of the overall number of detected burns and occurred mostly in forests. Because the purpose of this study is to observe the recovery of albedo and EVI in areas affected by fire, in the rare cases with two burns in a year, we chose to use only the last fire. Using the first burned pixel would provide a truncated estimate of recovery and thus not provide results that could be combined with the vast majority of pixels that burn only once in a year. This was done for years 2001 through 2015.

To obtain a single land-cover classification for the entire area, the most frequent IGBP vegetation class from 2000 to 2015 was chosen from MOD12Q2 pixels. For example, if a pixel was identified as cropland 10 times, and as grassland 5 times then the pixel was classified as cropland.

Average diurnal land surface albedo was estimated for all 16 day composites from 2000 to 2015 using the MODIS BRDF-Albedo Model Parameters (MCD43A1). The equation and coefficients provided by *Schaaf et al.* [2002] that provide the means to calculate black-sky albedo for a given solar zenith angle given pixel-specific BRDF-Albedo Model Parameters were used. For every pixel from 2000 to 2015, we estimated black-sky albedo hourly from 7 A.M. to 7 P.M., local time, based on the local solar zenith angle. The average of these values was used as the diurnal albedo for all further calculations.

Black-sky albedo and white-sky albedo mark the extreme cases of illumination from a single point and illumination from a constant-radiance hemisphere, respectively. The arid and semiarid systems of Africa are among the most cloud-free regions of the globe [e.g., *Wylie et al.*, 2005], meaning that they experience primarily direct solar illumination, as opposed to diffuse cloud-scattered illumination. For this reason, we have chosen to use black sky albedo for this analysis. A fuller treatment would use both black- and white-sky albedo weighted by the proportion of direct and diffuse illumination, but such an analysis is currently impossible because it would require diurnal measurements of diffuse versus direct illumination throughout the year on a continental scale. These data are not available.

A database of fires was produced by identifying all fires occurring in 500 m pixels across the study area for the period of 2000–2015 from the MOD45A1 data. For each fire pixel (i.e., a recorded fire in a particular year for a particular pixel), we extracted the albedo, EVI, and DSWRF from a period beginning 2 months before the fire and continuing until 9 months after the fire. This is the record of the fire in the year of the burn (YB). In addition, for each fire pixel we extracted albedo, DSWRF, and EVI for the full year beginning 14 months before the fire (the year before burn, YBB) and the full year beginning 10 months after the fire (the year after burn, YAB). This was done only for fires from 2001 to 2014 because MODIS data are only available from February 2000 onward.

For our analysis, we wished to compare the behavior of pixels that burned against control cases without fire. An inherent difficulty of this approach rests in the fact that an unburned pixel may have been burnable but may have lacked only conditions for ignition, in which case it is a good representation of the "control" case. However, some pixels may not be burnable even in the presence of ignition because of the state of the vegetation or other considerations. There is no approach using remote sensing data to differentiate clearly
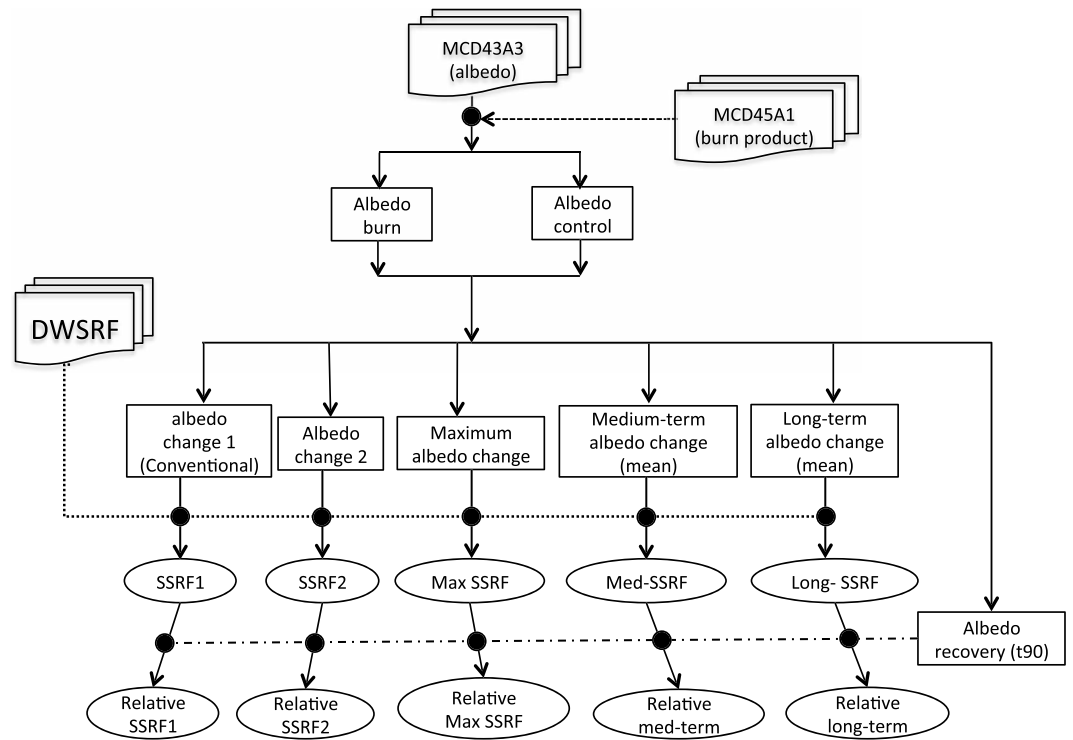
Figure 2. Flow chart of calculations of albedo change, surface shortwave radiative forcing (SSRF), and relative effect of radiative forcing over time. Solid circles represent the interaction between data sets.

between these two cases. We reasoned that a pixel in which fire does occur must, at least some of the time, exhibit conditions that make it burnable, as opposed to a neighboring pixel that may never be burnable. Thus, we conclude that a suitable comparison between burned and unburned pixels is a comparison of a burned pixel, in the year it burns, against itself, in nearby years it does not burn (year before burn, YBB, and year after burn YAB. Thus, provided that no fire occurs in the antecedent or subsequent year, the average of the YBB and YAB time series for fire pixels is used as the control for each fire pixel. Using both YBB and YAB allows the expression of some interannual variability for each pixel. This average is considered the control case and was calculated for all fire pixels for which it could be calculated (that is, for fire pixels in which the YBB is not before the beginning of the MODIS record, and fire pixels for which fire did not also occur in YBB or YAB).

The flowchart of albedo change, radiative forcing, and relative effect is illustrated in schematic diagram in Figure 2.

2.4. Fire-Induced Albedo (and EVI) Change

We calculated fire-induced albedo change for each pixel using YB (year of burn) and control data sets (that is, the average of YBB and YAB for each burn pixel). We calculated three types of albedo change. In the first approach, we calculated short-term albedo change (ΔA_1) using YB as outlined in equation (1). Short-term refers to 8 days, between the value recorded immediately before the burn (t_0) and the next available albedo value (t_1).

$$\Delta A_1 = a_{f\_t1} - a_{f\_t0} \tag{1}$$

where a_{f_t0} is the value of albedo at the time of burn and a_{f_t1} is the next albedo value after the burn in the same year. The ΔA_1 is the conventional method for calculating fire-induced albedo change, and it is commonly referred to as instantaneous albedo change [*Huang et al.*, 2014; *Jin et al.*, 2012; *Jin and Roy*, 2005; *López-Saldaña et al.*, 2014]. The different temporal components of equation (1), and subsequent equations, are illustrated in Figure 3.
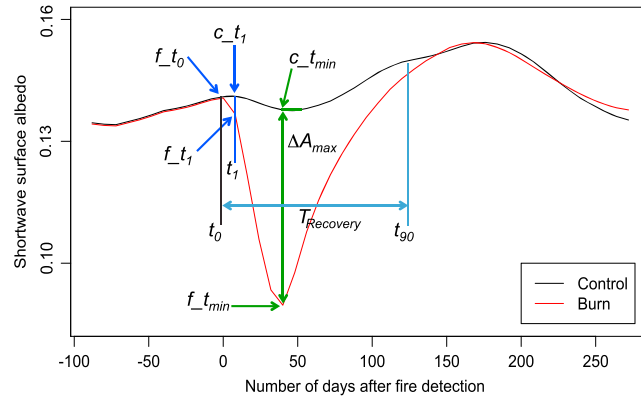
Figure 3. Illustration of the different components of the equations used in calculating albedo change. The notation "*f*" indicates the fire case and "*c*" indicates the control case. "*t*0" is the date of the fire. "*t*1" is the time of next image after fire. "*tmin*" is the time when the albedo of the fire case reaches a minimum, which also corresponds to the time when the difference between fire-case albedo and control case is at its maximum. "*t*90" is the time when the fire-case albedo has recovered to 90% of the control-case albedo. The time between $t0$ and tmin is defined as "medium-term" albedo change. The time between $t0$ and $t90$ is defined as "long-term" albedo change.

We calculated another short-term albedo change (ΔA_2) using YB and YAB data sets as outlined in equation (2).

$$\Delta A_2 = a_{f\_t1} - a_{c\_t1} \qquad (2)$$

where a_{c_t1} is the value of albedo in the control data set. Albedo change in ΔA_2 is the difference between burnt albedo in the year when there was fire, and control albedo the following year.

To calculate maximum albedo change (ΔA_{max}), we located the lowest albedo value after fire occurrence (a_{f_tmin}) in the YB data set, and located the value at the same time in the control data set (a_{c_tmin}). t_{min} is the time after the burn where the albedo of the burned pixel reaches its lowest value. We calculated the difference between the two values as shown in equation (3).

$$\Delta A_{max} = a_{f\_t\,min} - a_{c\_t\,min} \qquad (3)$$

For example, if the minimum postfire albedo, a_{f_tmin}, occurred in 31 October, then a_{c_tmin} would also be extracted for 31 October in the control case for that pixel.

To determine the length of time that fire affected surface reflectance, we calculated albedo recovery time ($T_{recovery}$). Albedo was considered recovered when the difference between burn albedo (a_{burn}) and control albedo ($a_{control}$) recovered to within 90% of its maximum absolute value. To calculate recovery time, we subtracted burn date (t_0) from the date when albedo was deemed recovered (t_{90}):

$$T_{recovery} = (t_{90}) - (t_0) \qquad (4)$$

This approach takes into account natural phenology because a burned pixel is monitored over time for a period of one full year. Thus, the natural phenological changes that occur throughout the year for both the burned and control cases are intrinsically included in the analysis.

2.5. Surface Shortwave Radiative Forcing Due To the Impact of Fire

Surface shortwave radiative forcing (SSRF) due to only fire was calculated by multiplying albedo change by associated surface incoming solar radiation $\left(I^{\downarrow}_{burn}\right)$, derived from DSWRF. We calculated SSRF$_1$ and SSRF$_2$ using ΔA_1 and ΔA_2, respectively, using equation (5):

$$SSRF_{1,2} = -\left(I^{\downarrow}_{burn} * \Delta A_{1,2}\right) \qquad (5)$$

We also calculated medium-term SSRF (SSRF$_{tmin}$) and long-term SSRF (SSRF$_{t90}$). The SSRF$_{tmin}$ was calculated by averaging the SSRF values from individual 16 day composites between time of burn and when albedo reached its minimum value at t_{min}. The same approach was used to calculate long-term SSRF (SSRF$_{long}$), where i is time when albedo was deemed recovered:

$$SSRF_{med,long} = -\frac{1}{N} \sum_{i=0}^{t_{min}\ or\ t_{90}} I_{t,i}\left(a_{f-t,i} - a_{c\_t,i}\right) \qquad (6)$$

Table 2. Fire-Induced Albedo Change (Mean ± SD)[a]

Region	IGBP Vegetation Type	Mean Annual Burn Area ($\times 10^3$ km^2)	Albedo Change		
			Short-Term 1	Short-Term 2	Maximum Change
			$(\alpha_{f\_t1} - \alpha_{f\_t0})$	$(\alpha_{f\_t1} - \alpha_{c\_t1})$	$(\alpha_{f\_tmin} - \alpha_{c\_tmin})$
NSSA	Savanna	746.9	−0.010 ± 0.014	−0.018 ± 0.013	−0.021 ± 0.012
	Shrubland	48.6	−0.019 ± 0.022	−0.038 ± 0.027	−0.039 ± 0.028
	Grassland	5.8	−0.021 ± 0.023	−0.048 ± 0.039	−0.048 ± 0.043
	Cropland	74.7	−0.011 ± 0.017	−0.023 ± 0.021	−0.026 ± 0.021
SHA	Savanna	678.2	−0.014 ± 0.016	−0.024 ± 0.012	−0.027 ± 0.011
	Shrubland	32.9	−0.015 ± 0.016	−0.035 ± 0.016	−0.039 ± 0.016
	Grassland	14.6	−0.015 ± 0.015	−0.029 ± 0.014	−0.033 ± 0.014
	Cropland	18.4	−0.016 ± 0.017	−0.026 ± 0.015	−0.026 ± 0.016
SSA	Savanna	1425.0	−0.013 ± 0.015	−0.022 ± 0.013	−0.024 ± 0.012
	Shrubland	20.3	−0.016 ± 0.018	−0.035 ± 0.018	−0.039 ± 0.019
	Grassland	81.5	−0.019 ± 0.021	−0.041 ± 0.033	−0.042 ± 0.036
	Cropland	93.1	−0.012 ± 0.017	−0.024 ± 0.02	−0.026 ± 0.02

[a]The short-term 1 was calculated using burn albedo, while short-term 2 and maximum change were calculated using burn and control albedo.

where i is time after burn, $I_{t,i}$ is the incoming solar radiation, and N is the number of 16 day composites that comprise t_{min} or t_{90}.

Because different approaches to calculating radiative forcing presented here have different temporal scales (instantaneous, t_{min}, or t_{90}), the energetic effect of each (J m^{-2}) differs even in cases where the radiative forcing (W m^{-2}) is the same. In order to make them comparable on an energetic basis, we introduce the concept of "*relative radiative forcing*." Relative radiative forcing is the radiative forcing that would need to operate over a certain reference period of time, here t_{90}, to provide a total radiative forcing equivalent that over which radiative forcing is actually calculated. If radiative forcing were time invariant, or as in our case, time-averaged, this can be expressed as $t_{ref} \cdot \text{RRF} = t_{calc} \text{SSRF}$, which can be rearranged to give $\text{RRF} = t_{calc}/t_{ref} * \text{SSRF}$. Because the reference time is t_{90}, in the long-term case, SSRF_{long}, relative radiative forcing equals the calculated radiative forcing.

3. Results

First, our results indicated that shrubland pixels behaved very similarly to savanna pixels whereas the behavior of grassland pixels differed significantly. Therefore, for the purpose of clarity, we omit shrubland results in the figures and the ensuing discussion, but do show the results for all biomes in the tables.

3.1. Fire Regime and Environmental Variables

Our analysis indicates that more than 90% of the fires occurred in the dry season in both regions. In NSSA the dry season occurs November to March, whereas in SHA the dry season occurs in May to October. In our analysis, most fires occurred in areas receiving between 300 mm and 1500 mm mean annual precipitation (MAP), with the largest frequency of fires occurring at 800–1200 mm MAP in both NSSA and SHA. About 22% and 12% of savannas burned annually in our analysis in the NSSA and SHA, respectively (Table 1). In grasslands, 2% and 5% burned annually in NSSA and SHA, respectively. At the continental scale, savanna and grassland fires covered 9.9% and 0.5% of SSA, respectively.

3.2. Fire-Induced Albedo

In all cases ΔA was negative. In NSSA grasslands had the largest ΔA_1 (instantaneous albedo change) than other ecosystems, whereas in SHA, croplands experienced the largest ΔA_1 (Table 2). In each region, savannas had the smallest ΔA_1. For ΔA_2 and ΔA_{max}, grasslands in NSSA had the largest values compared to other ecosystems, whereas in SHA, shrublands had the highest values. The variability for albedo change, represented by the standard deviation in Table 2, was an order of magnitude less than the associated mean albedo change values.
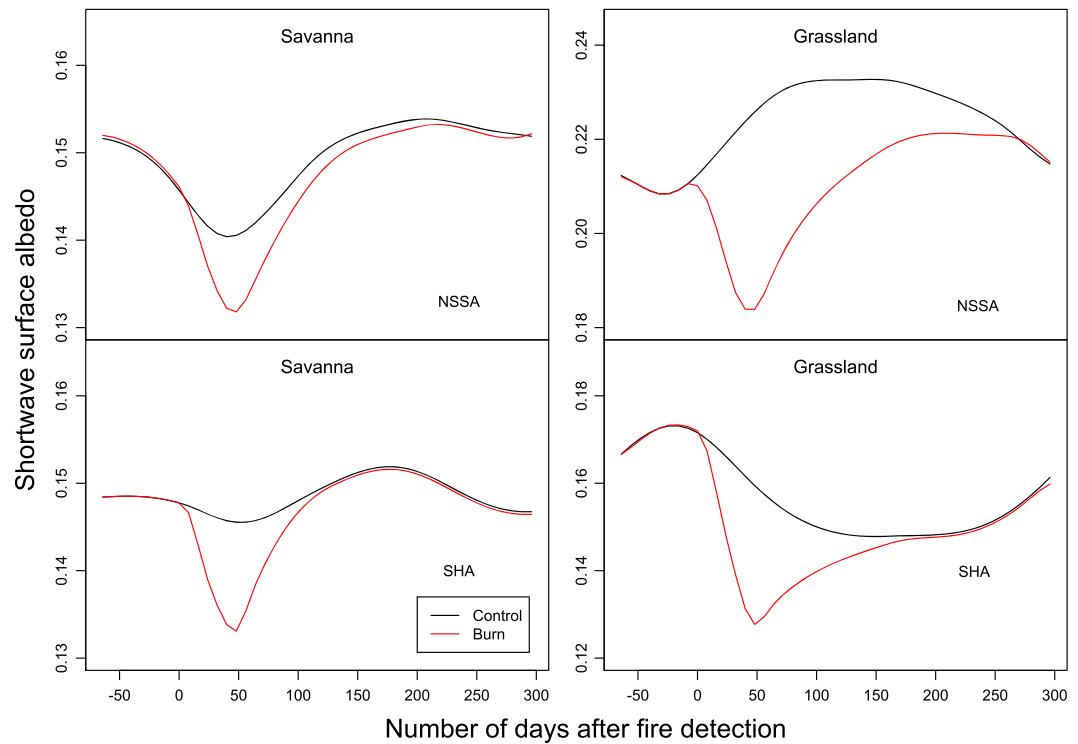
Figure 4. Average of shortwave surface albedo for burn (red) and control (black) cases for savannas and grasslands of NSSA and SHA. These lines represent the average across all fire pixels for the two cases starting 2 months before each fire and continuing for a full year. Negative values on the *x* axis represent preburn values and show good agreement between the burn and control cases before the burn.

3.3. Prefire and Postfire Albedo and EVI Patterns

In both NSSA and SHA, the 2 month prefire values of both the control and burn albedo curves are nearly the same (Figure 4). On average, after fire occurrence, the albedo of burned pixels dropped to a minimum after approximately 7 weeks and recovered (t_{90}) after ~18 weeks (Table 3). The behavior of NSSA grassland pixels differed from that of NSSA/SHA savannas and SHA grasslands pixels. For instance, control albedo in NSSA grassland pixels increased during the dry (fire) season, whereas control albedo decreased in other ecosystems. Recovery time in NSSA grassland pixels exceeded 250 days, whereas other classes recovered in significantly shorter times.

Table 3. Median Number of Days From the Date of Burn Per Treatment[a]

| | | Median Number of Days per Observation | | | | | |
| | | Short-term | | Maximum Change (t_{min}) | | Recovery (t_{90}) | |
Treatment	Region	t_1 (1)	t_1 (2)	Albedo	EVI	Albedo	EVI
NSSA	Savanna	8 ± 0	8 ± 0	48 ± 60	16 ± 26	128 ± 22	56 ± 21
	Shrubland	8 ± 0	8 ± 0	32 ± 63	32 ± 27	>240	>200
	Grassland	8 ± 0	8 ± 0	24 ± 70	24 ± 27	>200	>200
	Cropland	8 ± 0	8 ± 0	40 ± 74	16 ± 26	184 ± 24	80 ± 19
SHA	Savanna	8 ± 0	8 ± 0	48 ± 52	16 ± 39	128 ± 23	64 ± 27
	Shrubland	8 ± 0	8 ± 0	16 ± 40	16 ± 40	>248	> 200
	Grassland	8 ± 0	8 ± 0	16 ± 60	24 ± 37	> 240	80 ± 17
	Cropland	8 ± 0	8 ± 0	40 ± 79	32 ± 36	200 ± 19	120 ± 36

[a]t_1 represents the number of days after burn and the next observation, while t_{min} and t_{90} represent the number of days it takes for albedo and EVI change to reach maximum and 90% recovery, respectively. Uncertainty represents standard deviations.
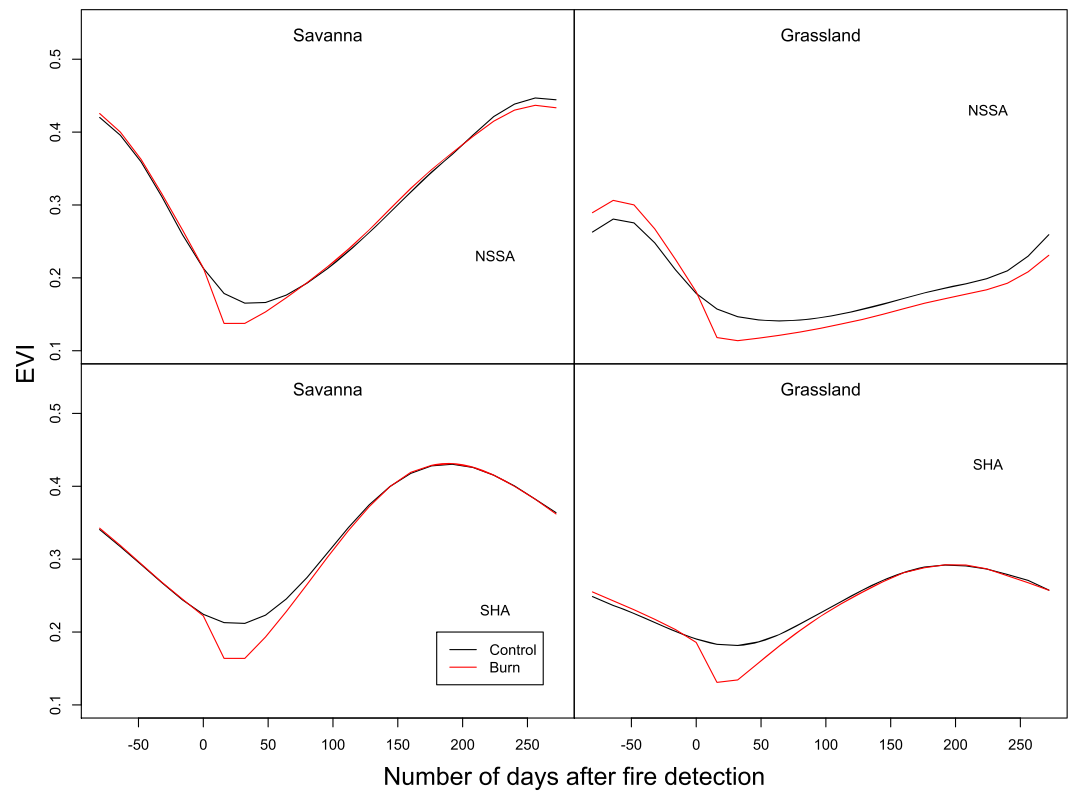
Figure 5. Same as Figure 4, except showing EVI instead of albedo.

Savannas took a longer time, compared to other vegetation classes, for postfire albedo to reach the minimum (t_{min}), while grasslands took the shortest time (Table 3). In savannas, t_{90} was shorter than grasslands (Table 3). The weighted average of recovery times (t_{90}) for burns across Africa is 138 days or ~40% of a year.

For EVI, the burn and the control values in the savannas were nearly the same before burns, after which burn case EVI values decreased (Figure 5), reaching the minimum value in about 16 days (Table 3). After the drop, the savanna burn EVI values remained low and constant for about 2 weeks and then started to increase for

Table 4. Surface Shortwave Radiative Forcing (Mean ± SD) Exerted Due To Fires[a]

			Shortwave Surface Radiating Forcing (W m^{-2})				
			Short-Term SSRF1	Short-Term SSRF2	SSRF-max	Average Medium-Term	Average Long-Term
Region	IGBP Vegetation Type	Mean Annual Burn Area (× 10^3 km^2)	$I(\alpha_{f\_t1} - \alpha_{f\_t0})$	$I(\alpha_{f\_t1} - \alpha_{ct1})$	$I(\alpha_{f\_tmin} - \alpha_{c\_tmin})$	$1/N \sum_{i=0}^{t\,min} I_{ti}(a_{fti} - a_{cti})$	$1/N \sum_{i=0}^{t90} I_{ti}(a_{fti} - a_{cti})$
NSSA	Savanna	746.9	2.55 ± 3.74	3.83 ± 3.98	4.48 ± 3.75	4.05 ± 3.86	2.91 ± 2.78
	Shrubland	48.6	5.37 ± 7.98	11.08 ± 17.77	11.89 ± 24.77	11.39 ± 20.33	7.03 ± 9.50
	Grassland	5.8	5.47 ± 7.51	13.37 ± 18.57	13.47 ± 25.95	13.43 ± 21.25	8.01 ± 9.60
	Cropland	74. 7	3.1 ± 6.18	6.01 ± 10.72	6.68 ± 14.19	6.28 ± 11.92	4.18 ± 6.40
SHA	Savanna	678.2	3.88 ± 5.97	5.58 ± 4.99	6.17 ± 5.04	5.66 ± 4.89	4.08 ± 4.00
	Shrubland	32.9	4.42 ± 6.12	11.01 ± 7.48	10.33 ± 6.88	11.78 ± 7.93	6.37 ± 4.91
	Grassland	14.6	4.34 ± 5.79	8.23 ± 6.38	8.15 ± 6.04	8.72 ± 6.67	5.03 ± 4.38
	Cropland	18.4	5.1 ± 9.45	8.33 ± 11.65	8.48 ± 11.34	8.3 ± 12.18	5.77 ± 8.02
SSA	Savanna	1425.0	3.35 ± 5.23	4.90 ± 4.70	5.52 ± 4.65	5.04 ± 4.58	3.63 ± 3.62
	Shrubland	20.3	4.62 ± 6.55	11.02 ± 10.37	10.64 ± 12.65	11.70 ± 11.51	6.5 ± 6.10
	Grassland	81.5	5.07 ± 6.96	11.49 ± 15.48	11.53 ± 21.14	11.71 ± 17.55	6.92 ± 8.22
	Cropland	93.1	3.52 ± 7.03	6.46 ± 10.94	7.03 ± 13.70	6.67 ± 11.99	4.49 ± 6.77

[a]I and N represent the incident surface incoming solar radiation (W m^{-2}) and the number of samples per observation, respectively.
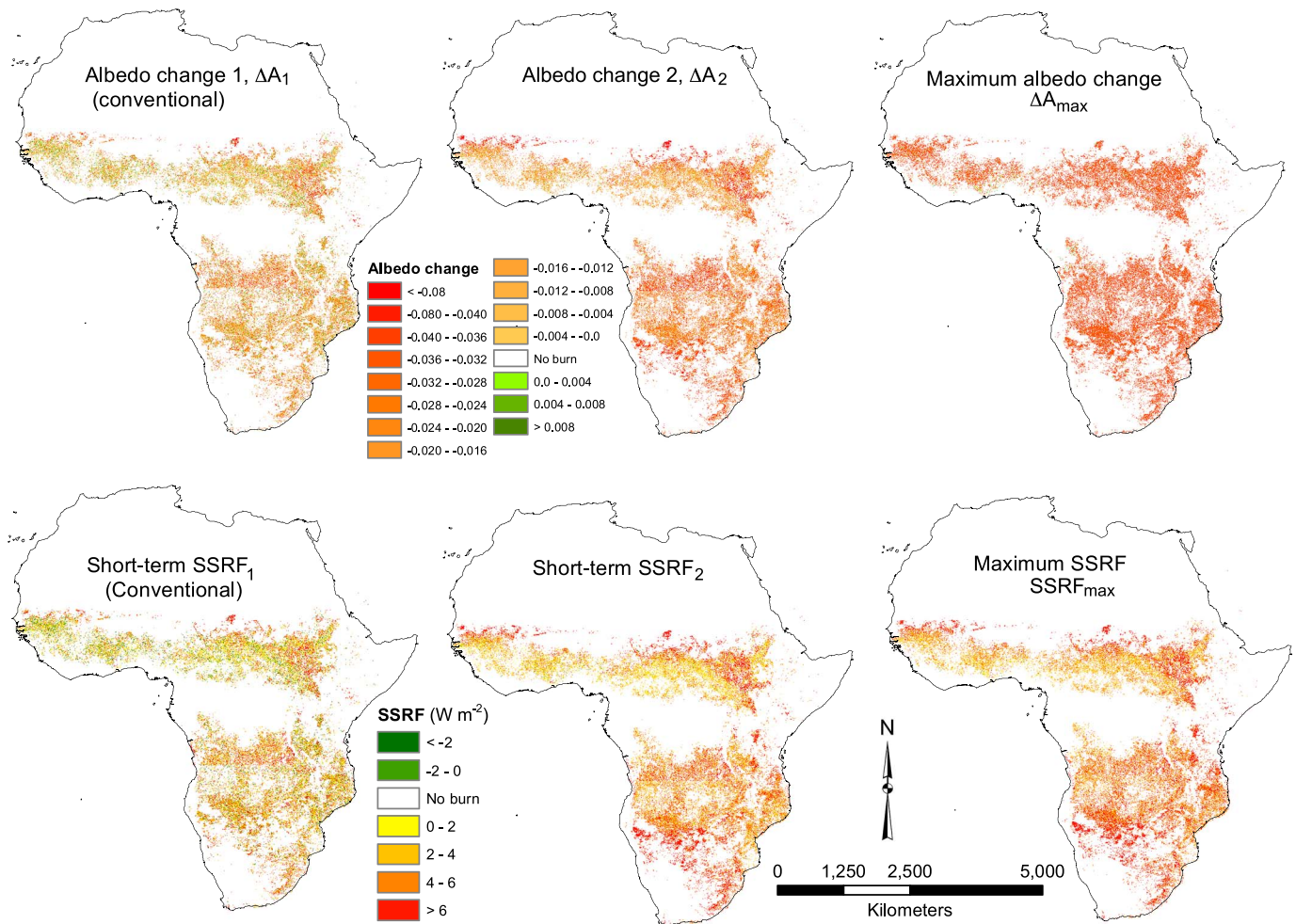
Figure 6. Spatial distribution of albedo change and associated radiative forcing over Africa.

4 weeks, until they returned nearly to the control values. In the grasslands, burn-EVI values started slightly higher than the control, with the NSSA showing a considerable difference (Figure 5). The burn-EVI values in grasslands reached a minimum about 24 days after the fire (Table 3) and remained constant for about 2 weeks after burn, and then started to recover. In SHA, grasslands the burn-EVI reached control values upon recovery, whereas in NSSA burn-EVI values never reached control values. Post-fire EVI recovery was faster in savannas than in other vegetation classes.

3.4. Radiative Forcing Due To Fire-Induced Albedo Change

In all cases, average radiative forcing was positive (Table 4). The short-term-1 radiative forcing (SSRF1) exerted by fire-induced albedo change was greatest in grasslands and least in savannas in NSSA, whereas in SHA, croplands experienced the greatest SSRF1 and savannas experienced the least SSRF1, respectively. In NSSA, SSRF2 was greatest in grasslands, whereas in SHA it was greatest in shrublands. Similarly, maximum radiative forcing (SSRFmax), medium-term and long-term SSRF were greatest in grasslands in NSSA and SHA, respectively. Variability (standard deviations in Table 4) for radiative forcing were of the same order of magnitude as the associated mean values indicating significant continental-scale variability in radiative forcing response related to latitude; because albedo change was lowest near the equator and highest away from the equator in both subregions of Africa, the associated radiative forcing followed a similar pattern, exacerbated by variability in solar irradiance (Figure 6).

Table 5. Relative Effect of Fire-Induced Surface Shortwave Radiative Forcing (Mean ± SD)[a]

Region	IGBP Vegetation Type	Mean Annual Burn Area $(\times 10^3 \text{ km}^2)$	Relative Effect of Fire-Induced Shortwave Surface Radiating Forcing (W m^{-2})				
			Short-Term SSRF1 $I/t_{90}[a_{f\_t0} - a_{f\_t0}]$	**Short-Term SSRF2** $I/t_{90}[a_{f\_t1} - a_{f\_t1}]$	**Maximum SSRF** $t_{min}/t_{90}I[a_{f\_t1} - a_{f\_t1}]$	**Medium-Term** $1/N\sum_{i=o}^{t\,min}\frac{t_{min}}{t_{90}}I(a_{fti} - a_{cti})$	**Long-Term** $1/N\sum_{i=0}^{t90}I_{ti}(a_{fti} - a_{cti})$
NSSA	Savanna	746.9	0.16 ± 0.23	0.24 ± 0.24	1.65 ± 1.38	1.50 ± 1.42	2.91 ± 2.78
	Shrubland	48.6	0.18 ± 0.27	0.37 ± 0.59	1.58 ± 3.30	1.52 ± 2.71	7.03 ± 9.50
	Grassland	5.8	0.22 ± 0.30	0.53 ± 0.74	1.62 ± 3.11	1.61 ± 2.55	8.01 ± 9.60
	Cropland	74.7	0.14 ± 0.27	0.27 ± 0.48	1.48 ± 3.15	1.40 ± 2.65	4.18 ± 6.40
SHA	Savanna	678.2	0.24 ± 0.37	0.34 ± 0.31	2.28 ± 1.86	2.09 ± 1.81	4.08 ± 4.00
	Shrubland	32.9	0.15 ± 0.20	0.37 ± 0.25	0.69 ± 0.46	0.79 ± 0.53	6.37 ± 4.91
	Grassland	14.6	0.14 ± 0.19	0.26 ± 0.20	0.52 ± 0.39	0.56 ± 0.43	5.03 ± 4.38
	Cropland	18.4	0.20 ± 0.38	0.33 ± 0.47	1.70 ± 2.27	1.66 ± 2.44	5.77 ± 8.02
SSA	Savanna	1425.0	0.21 ± 0.32	0.30 ± 0.29	2.04 ± 1.72	1.86 ± 1.69	3.63 ± 3.62
	Shrubland	20.3	0.15 ± 0.22	0.37 ± 0.35	1.06 ± 1.27	1.17 ± 1.15	6.50 ± 6.10
	Grassland	81.5	0.18 ± 0.25	0.41 ± 0.55	1.02 ± 1.88	1.04 ± 1.56	6.92 ± 8.22
	Cropland	93.1	0.15 ± 0.30	0.27 ± 0.46	1.48 ± 2.88	1.40 ± 2.53	4.49 ± 6.77

[a]I and N represent the incident surface incoming solar radiation (W m^{-2}) and the number of samples per observation, respectively.

3.5. Implication of Medium- and Long-Term SSRF on Energy Balance

Relative radiative forcing increased with time (that is, from instantaneous to t_{min} to t_{90}) in all the ecosystems (Table 5). For example, in NSSA savannas, the relative SSRF effect was 0.16 ± 0.23, 0.24 ± 0.24, 1.50 ± 1.42, and 2.91 ± 2.78 W m^{-2} for R_{s1}, R_{s2}, R_{med}, and R_{long} respectively. Variability in relative radiative forcing, represented by the standard deviation in Table 5, reflects variability in the radiative forcing (Table 4).

To determine the mean regional contribution of burn-related SSRF1 for NSSA we multiplied this forcing by the proportion of the total burn area to the total regional land area, which gave mean regional SSRF1 of 0.09 W m^{-2} (Table 6). Performing similar analysis for SHA and SSA we found mean regional SSRF1 of 0.30 and 0.16 W m^{-2} for SHA and SSA, respectively. Performing the same analysis using SSRF2, we calculated mean regional SSRF2 to be 0.16, 0.46, and 0.25 W m^{-2} for NSSA, SHA, and SSA, respectively.

At continental scale, the weighted mean relative effect of SSRF was 0.20, 0.30, 1.78, and 3.88 W m^{-2} for R_{s1}, R_{s2}, R_{med} , and R_{long}, respectively (Figure 7). At regional scale SHA experienced the highest weighted relative SSRF effect compared to NSSA in all the treatments. In this analysis, we found that R_{long} and R_{med} effects were an order of magnitude greater than R_{s1}, R_{s2}, with the long-term showing greatest effects.

We further calculated the global contribution to radiative forcing exerted by fires in Africa. Assuming the global land surface area of 150×10^6 km^2, we calculated that the annual burn area in Africa was 1.6×10^6 km^2 and constituted 1.1% of the global land surface area. Multiplying the SSRF1 for SSA by 1.1% suggests that fires in Africa contributed at least a radiative forcing of 0.037 W m^{-2} globally. Using the more new value of SSRF2 for SSA, we conclude that the short-term global radiative forcing of fires in SSA is 0.058 W m^{-2}.

Table 6. The Weighted Mean of SSRF (W m^{-2}, Weighted by the Contributions of Vegetation Type to Burn Area) and the Mean Regional (i.e., NSSA, SHA, and SSA) Radiative Forcing (Mean ± SD)[a]

Region	Weighted Mean	Short-Term SSRF1	Short-Term SSRF2	Maximum SSRF	Medium-Term SSRF	Average Long-Term SSRF
NSSA	SSRF in burned areas	2.78 ± 4.19	4.60 ± 5.46	5.22 ± 6.02	4.81 ± 5.63	3.33 ± 3.52
SHA		3.96 ± 6.08	5.97 ± 5.37	6.48 ± 5.36	6.10 ± 5.33	4.26 ± 4.18
SSA		3.46 ± 5.44	5.41 ± 5.68	5.98 ± 6.12	5.56 ± 5.76	3.88 ± 4.07
NSSA	Regional	0.09 ± 0.14	0.16 ± 0.19	0.18 ± 0.20	0.16 ± 0.19	0.11 ± 0.12
SHA	Regional	0.30 ± 0.47	0.46 ± 0.41	0.50 ± 0.41	0.47 ± 0.41	0.33 ± 0.32
SSA	Continental	0.16 ± 0.25	0.25 ± 0.26	0.27 ± 0.28	0.25 ± 0.26	0.18 ± 0.19

[a]The mean regional radiative forcing was calculated by multiplying the regional weighted-mean SSRF by the proportion of each region's land area that is burned (from Table 1).
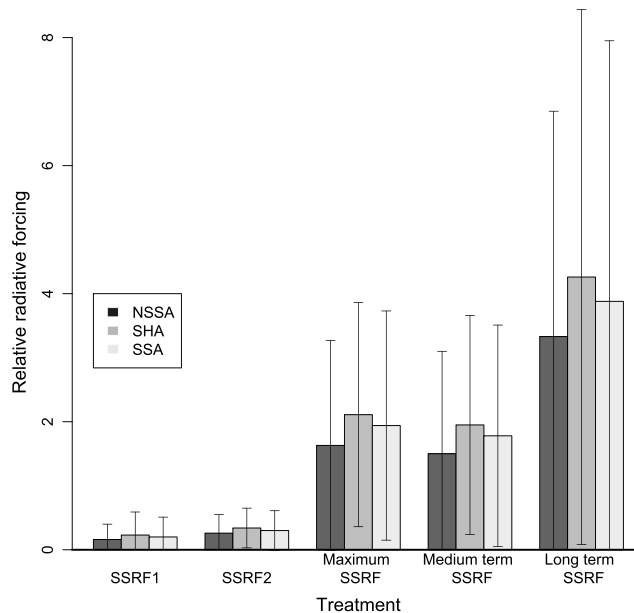
Figure 7. The relative effect of surface shortwave radiative forcing calculated over short (SSRF1 and SSRF2), medium (maximum SSRF and medium-term SSRF), and long (long-term SSRF) time frames.

4. Discussion

4.1. Fire-Induced Albedo Change and Vegetation Structure

The difference between albedo patterns in NSSA and SHA savannas could be attributed to vegetation structure and composition (Figure 1). In NSSA the dominant tree species are deciduous *Acacias*, which lose their leaves during the dry season, whereas in SHA there is a great variety in vegetation composition ranging from deciduous acacias in the south to broadleaf-evergreen trees in the north [*Caylor et al.*, 2003; *Scholes et al.*, 2002].

In NSSA, the postfire short-term shortwave albedo decreased by 0.010 and 0.021 in savannas and grasslands, respectively, whereas in SHA it decreased by 0.014 and 0.155 in savannas and grassland, respectively (Table 2). Our results are consistent with results from northern Australia where albedo decrease was higher in grassland than woodland savannas [*Jin and Roy*, 2005]. One of the reasons why grasslands experienced a greater decrease in albedo could be due to the amount of fuel load and the type of fire. Grasslands tend to form a continuous carpet, which facilitates the spread and increase fire intensity [*Romero-Ruiz et al.*, 2010]. In savannas, the discontinuous grass carpet reduces fire spread and intensity. Grasses usually experience complete combustion whereas shrubs and trees only partially burn. *van Altena et al.* [2012] showed that there was a positive correlation between species flammability and fire severity. Similarly, *Amraoui et al.* [2010] suggested that vegetation type in sub-Saharan Africa regulated fire activity. Biomass combustion resulted in grasslands covered by continuous black-gray residues, whereas in savannas the surface was covered by discontinuous black-gray residue and bare soil patches. As a result, we conclude that vegetation (and hence, land cover type) plays an important role in influencing postfire albedo pattern.

4.2. Postfire Albedo and EVI Recovery

We observed that postfire albedo continued to decrease for couple of weeks before the recovery (Figure 4). We expected albedo to drop abruptly in the first week (8 days) and to remain constant for a few weeks before recovery. The reason why postfire albedo continued to drop could be that the residues were not translocated to another place by aeolian or hydrological process, but rather they remain on the same place. *De Sales et al.* [2015] suggested that in NSSA postfire albedo would decrease abruptly, and then increase above the control values as a result of exposing bare soil due to vegetation deterioration and ash being translocated to other places. However, our results showed that postfire albedo did not increase above control values. The fact that albedo recovery did not generally exceed control values suggests that albedo recovery was a function of vegetation recovery and was not influenced by bare soil patches. For bare soil patches to be fully exposed there has to be strong winds or substantial runoff post fire, but in these systems with strong wet-dry seasonality, rains typically start abruptly at the beginning of the wet season, when we saw albedo recover for other reasons, like leaf bud. Furthermore, we do not expect fire-prone ecosystems to have large intercanopy spaces (otherwise, fire would not spread) that would expose a bright soil background. Therefore, we suggest that continued postfire albedo decreases are the result of charcoal or other dark residues being translocated locally into bare soil patches between plant canopies, thus darkening the overall surface for a period of time. Ash from burning of woody material initially is bright and highly transportable by wind. When it is translocated to the soil and wetted or flattened, it becomes dark.

Postfire EVI recovered faster than albedo in NSSA and SHA regardless of vegetation type (Table 3). This pattern supports the idea that vegetation recovery was prerequisite for albedo recovery [*Pinty et al.*, 2000; *Tsuyuzaki et al.*, 2009]: as vegetation recovers, the contribution of exposed bright soil surfaces, charcoal, ash, and other dark residues decreases and the overall albedo begins to reflect the albedo of vegetation. Postfire EVI in grasslands took longer to recover compared to savannas, which possibly reflected combustion intensities in the two ecosystems. Grasslands tend to experience surface fires, which are more intense and severe than those in savannas [*Bowman et al.*, 2009; *Viegas*, 2002]. Similar observations were made in Northern Australia where severe and intense fires resulted in longer recovery times, whereas less intense fires resulted in shorter vegetation (EVI) and albedo recovery time [*Beringer et al.*, 2003].

There is an inconsistency among studies in estimates of fire-induced albedo change. For example, *Gatebe et al.* [2014] estimated albedo change in NSSA savannas to be −0.0022, which is an order of magnitude lower than our result suggests. The discrepancy could largely be attributed to the methods used in the studies. *Gatebe et al.* [2014] used unburned neighboring pixels as control, whereas in our study we compared a pixel to itself (equations (2) and (3)) in neighboring year where it did not burn. The approach of comparing two neighboring pixels is commonly used [e.g., *Gatebe et al.*, 2014; *Huang et al.*, 2014; *Lyons et al.*, 2008; *Myhre et al.*, 2005; *Samain et al.*, 2008], but it does not take into account heterogeneity of the land surface. That is, it assumes homogenous vegetation cover. Neighboring pixels do not necessarily represent a comparable vegetation state, and the fact that the adjacent pixel did not burn could be an indication that the vegetation types and prevailing environmental conditions in the two pixels were different. When we used the neighboring pixels method, the burn and control curves did not line up in the preburn period (versus Figure 4), indicating that they were not a good proxy (not shown). Our method (equations (2) and (3)) also took into account temporal change in unburned systems. To the best of our knowledge, no previous studies have done this. We have shown that calculating fire-induced albedo change using the conventional method (equation (1)) results in much lower values compared to equation (2). Going a step further to calculate maximum albedo change (equation (3)), the albedo differences were more than double those obtained using the neighbor method. These three sets of results clearly show that calculating fire-induced albedo change using the typical neighboring-pixel approach potentially underestimates the impact of fire, which in many cases has led to the conclusion that fire-induced albedo change is insignificant and less important to energy balance [e.g., *Gatebe et al.*, 2014] than our results suggest.

4.3. Fire-Induced Surface Shortwave Radiative Forcing

The concept of radiative forcing has been widely used to evaluate and compare the strength of the various factors affecting the Earth's radiation balance, and how they influence climate change [*Myhre et al.*, 2013]. In this study, we have presented four different methods of calculating radiative forcing.

When we used the conventional method (equation (5)), grasslands had the highest SSRF1 compared to other ecosystems. Savannas had the lowest SSRF1. Similar results were found in northern Australia where SSRF1 in savannas was lower than in grasslands *Jin and Roy* [2005]. However, more than 80% of the burn area in our study occurred in savanna ecosystems; therefore, the overall radiative forcing due to savannas plays an important role in the regional and continental scales. In SSA, the SSRF1 in burned areas was 3.46 W m^{-2} with a contribution continent (SSA) wide of 0.16 W m^{-2} (Table 6) For comparison, *Myhre et al.* [2005] reported that biomass burning overall exerted SSRF1 of 0.10 W m^{-2} on the African continent. *Myhre et al.* [2005] further reported a maximum SSRF of 8.00 W m^{-2} due to biomass burning. Our results indicated a similar value of 5.98 W m^{-2}. In Australia, *Jin and Roy* [2005] calculated the regional and continental SSRF1 to be 1.18 and 0.52 W m^{-2} for northern Australia and continental Australia, respectively, which are higher than the values reported here for SSA (0.09–0.16 W m^{-2}; Table 6).

When we calculated the difference between burn-albedo and control, SSRF2 was about 30% greater than SSRF1. Because burn and albedo data were the same for the SSRF1 and SSRF2 calculations, the difference in the results can be attributed only to the difference between control data and albedo data at—and after—the time of burn. We also found that maximum SSRF, which occurred when burn-albedo reached minimum value, was at least 80% greater than SRRF1 and SSRF2 in all the land cover types investigated here. Our results suggest that the conventional method (SSRF1) considerably underestimates the effect of fire on surface energy balance, and they further highlight the importance of considering temporal variability when assessing radiative forcing exerted by fires.

4.4. Implication of Medium- and Long-Term SSRF on Energy Balance

We calculated that fires in SSA contributed a radiative forcing of 0.16 and 0.25 W m^{-2} for SSRF1 and SSRF2, respectively (Table 6). Scaling to the Earth's land surface, African fires contributed radiative forcing of 0.037 and 0.058 W m^{-2} for SSRF1 and SSRF2, respectively. These global estimated contributions are higher than the global mean radiative forcing due to fire of 0.028 W m^{-2} reported by *López-Saldaña et al.* [2014], whose estimate also includes negative forcing due to fire in boreal forests as well as fires in other regions of the world.

Our calculated radiative forcings are generally within a factor of 2 to 3, with medium- and long-term radiative forcing always exceeding SSRF1 (Table 4). But, we found that the medium- and long-term *relative* radiative forcings due to fire were an order of magnitude greater than short-term effects (SSRF1 and SSRF2; Table 5) due to their longer duration; the area-weighted average of the ratio of long-term relative radiative forcing to relative SSRF is 19. Therefore, the real energetic effect of fire in these dryland systems, integrating over time, is roughly 20 times greater than what would be expected if only short-term estimates are made.

5. Conclusions

Because our results showed that fire had long-lasting effects of surface albedo (Figure 4), we derived a method to calculate the relative effect of surface shortwave radiative forcing at different time scales. Our results show that the relative effect of SSRF increased with time (Figure 7). This effect is, of course, not constant throughout a year and therefore cannot be compared directly with constantly present radiative forcings such as those due to CO_2 and other greenhouse gasses.

Nonetheless, a simple calculation of the global contribution to the Earth's radiative forcing can be made, taking into account the duration of fire-derived albedo effects. Our estimated mean short-term (SSRF2) radiative forcing for SSA is 0.25 W m^{-2} (Table 6). On an area-weighted basis, the average long-term relative radiative forcing is ~19 times that of the short-term relative radiative forcing (from Table 5). Further, in both NSSA and SHA, the area-weighted recovery time (t_{90}) is at least 140 days, which is ~40% of a year (from Table 3). Thus, by multiplying the estimated mean short-term radiative forcing for SSA (0.25 W m^{-2}) by (1) the effective increase in radiative forcing resulting from persistent burn scars (19), (2) the proportion of the year that this effect lasts (40%), and (3) the fraction of the Earth's surface occupied by Africa (6%), we conclude that the total radiative forcing contribution for African dryland fires globally across the entire year is at least 0.12 W m^{-2}. Calculated using the estimated short-term radiative forcing only, this result would be a factor of 19 smaller, or ~0.006 W m^{-2}.

Africa is the single largest continental source of burning biomass, with its fires responsible for about 50% of the total amount of area burned globally each year, and dryland fires, like those examined here comprise 75% of the Earth's burned area [*Roy et al.*, 2008]. The radiative effect of albedo change in dryland fires globally therefore could be as high as ~0.16 W m^{-2} (=0.12 W m^{-2}/75%). This is a significant result, indicating that global contribution of the albedo changes due to fires in drylands could be on the order of other important radiative forcings including anthropogenic N_2O (0.17 W m^{-2}), nonmethane volatile organic compounds (0.10 W m^{-2}), and albedo change due to land use (−0.15 W m^{-2}). This comparison is not meant to imply that all dryland fires are anthropogenic. Rather, it is meant to show that when the duration of the albedo effect of these fires is included, the resulting albedo changes have global significance. Excluding the duration of the fires, the calculated radiative forcing is much less significant.

A further component of fire's global effect is the gasses and aerosols produced during burning, which were not addressed here. The net radiative effect of these combustion products is likely positive [e.g., *Randerson et al.*, 2006], meaning that the radiative impact of fire from drylands is likely larger than is implied by the simple calculations presented here. A better accounting of these processes could help improve climate model projections, particularly on the issue of climate change and land-atmosphere feedback.

References

Amraoui, M., C. C. DaCamara, and J. M. C. Pereira (2010), Detection and monitoring of African vegetation fires using MSG-SEVIRI imagery, *Remote Sens. Environ.*, 114(5), 1038–1052, doi:10.1016/j.rse.2009.12.019.

Ångström, A. (1925), The albedo of various surfaces of ground, *Geogr. Ann.*, 7, 323–342, doi:10.2307/519495.

Archer, S., T. W. Boutton, and K. A. Hibbard (2001), Trees in grasslands: Biogeochemical consequences of woody plant expansion, in *Global Biogeochemical Cycles in the Climate System*, pp. 115–137, Academic Press, San Diego, Calif.

Belcher, C. M., J. M. Yearsley, R. M. Hadden, J. C. McElwain, and G. Rein (2010), Baseline intrinsic flammability of Earth's ecosystems estimated from paleoatmospheric oxygen over the past 350 million years, *Proc. Natl. Acad. Sci.*, *107*(52), 22,448–22,453, doi:10.1073/pnas.1011974107.

Beringer, J., L. B. Hutley, N. J. Tapper, A. Coutts, A. Kerley, and A. P. O'Grady (2003), Fire impacts on surface heat, moisture and carbon fluxes from a tropical savanna in northern Australia, *Int. J. Wildland Fire*, *12*(4), 333–340.

Bond, W. J., and J. E. Keeley (2005), Fire as a global 'herbivore': The ecology and evolution of flammable ecosystems, *Trends Ecol. Evol.*, *20*(7), 387–394, doi:10.1016/j.tree.2005.04.025.

Bond, W. J., F. I. Woodward, and G. F. Midgley (2005), The global distribution of ecosystems in a world without fire, *New Phytol.*, *165*(2), 525–537, doi:10.2307/1514732.

Bowman, D. M. J. S., et al. (2009), Fire in the Earth system, *Science*, *324*(5926), 481–484, doi:10.1126/science.1163886.

Cahoon, D. R., B. J. Stocks, J. S. Levine, W. R. Cofer, and K. P. O'Neill (1992), Seasonal distribution of African savanna fires, *Nature*, *359*(6398), 812–815, doi:10.1038/359812a0.

Caylor, K. K., H. H. Shugart, P. R. Dowty, and T. M. Smith (2003), Tree spacing along the Kalahari transect in southern Africa, *J. Arid Environ.*, *54*(2), 281–296, doi:10.1006/jare.2002.1090.

Cooke, W. F., B. Koffi, and J. M. Grégoire (1996), Seasonality of vegetation fires in Africa from remote sensing data and application to a global chemistry model, *J. Geophys. Res.*, *101*(D15), 21,051–21,065, doi:10.1029/96JD01835.

D'Odorico, P., F. Laio, A. Porporato, L. Ridolfi, and N. Barbier (2007), Noise-induced vegetation patterns in fire-prone savannas, *J. Geophys. Res.*, *112*, G02021, doi:10.1029/2006JG000261.

De Sales, F., Y. Xue, and G. S. Okin (2015), Impact of burned areas on the northern African seasonal climate from the perspective of regional modeling, *Clim. Dyn.*, *47* 1–21, doi:10.1007/s00382-015-2522-4.

Dickinson, R. E. (1983), Land surface processes and climate—Surface albedos and energy balance, in *Advances in Geophysics*, edited by B. Saltzman, pp. 305–353, Academic Press, New York, doi:10.1016/S0065-2687(08)60176-4.

Flannigan, M. D., M. A. Krawchuk, W. J. de Groot, B. M. Wotton, and L. M. Gowman (2009), Implications of changing climate for global wildland fire, *Int. J. Wildland Fire*, *18*(5), 483–507.

Friedl, M. A., D. Sulla-Menashe, B. Tan, A. Schneider, N. Ramankutty, A. Sibley, and X. Huang (2010), MODIS Collection 5 global land cover: Algorithm refinements and characterization of new datasets, *Remote Sens. Environ.*, *114*(1), 168–182, doi:10.1016/j.rse.2009.08.016.

Gatebe, C. K., C. M. Ichoku, R. Poudyal, M. O. Román, and E. Wilcox (2014), Surface albedo darkening from wildfires in northern sub-Saharan Africa, *Environ. Res. Lett.*, *9*(6), 065003, doi:10.1088/1748-9326/9/6/065003.

Giglio, L., J. Descloitres, C. O. Justice, and Y. J. Kaufman (2003), An enhanced contextual fire detection algorithm for MODIS, *Remote Sens. Environ.*, *87*(2–3), 273–282, doi:10.1016/S0034-4257(03)00184-6.

Glasspool, I. J., D. Edwards, and L. Axe (2004), Charcoal in the Silurian as evidence for the earliest wildfire, *Geology*, *32*(5), 381–383, doi:10.1130/G20363.1.

Govaerts, Y. M., J. M. Pereira, B. Pinty, and B. Mota (2002), Impact of fires on surface albedo dynamics over the African continent, *J. Geophys. Res.*, *107*(D22), 4629, doi:10.1029/2002JD002388.

Grace, J., J. S. José, P. Meir, H. S. Miranda, and R. A. Montes (2006), Productivity and carbon fluxes of tropical savannas, *J. Biogeogr.*, *33*(3), 387–400, doi:10.1111/j.1365-2699.2005.01448.x.

Hao, W. M., and M.-H. Liu (1994), Spatial and temporal distribution of tropical biomass burning, *Global Biogeochem. Cycles*, *8*(4), 495–503, doi:10.1029/94GB02086.

Hartmann, D. L., et al. (2013), Observations: Atmosphere and surface, in *Climate Change 2013: The Physical Science Basis. Contribution of Working Group I to the Fifth Assessment Report of the Intergovernmental Panel on Climate Change*, edited by T. F. Stocker et al., pp. 159–254, Cambridge Univ. Press, Cambridge, U. K., and New York.

Huang, S., D. Dahal, H. Liu, S. Jin, C. Young, S. Li, and S. Liu (2014), Spatiotemporal variation of surface shortwave forcing from fire-induced albedo change in interior Alaska, *Can. J. For. Res.*, *45*(3), 276–285, doi:10.1139/cjfr-2014-0309.

Huete, A. R. (2012), Vegetation indices, remote sensing and forest monitoring, *Geography Compass*, *6*(9), 513–532, doi:10.1111/j.1749-8198.2012.00507.x.

Intergovernmental Panel on Climate Change (2013), *Climate Change 2013: The Physical Science Basis. Working Group I contribution to the IPCC 5th Assessment Report*, 1552 pp., Cambridge Univ. Press, Cambridge, U. K.

Jin, Y., and D. P. Roy (2005), Fire-induced albedo change and its radiative forcing at the surface in northern Australia, *Geophys. Res. Lett.*, *32*, L13401, doi:10.1029/2005GL022822.

Jin, Y., J. T. Randerson, M. L. Goulden, and S. J. Goetz (2012), Post-fire changes in net shortwave radiation along a latitudinal gradient in boreal North America, *Geophys. Res. Lett.*, *39*, L13403, doi:10.1029/2012GL051790.

Knapp, A. K., et al. (2008), Consequences of more extreme precipitation regimes for terrestrial ecosystems, *Bioscience*, *58*(9), 811–821, doi:10.1641/B580908.

Liu, Z., D. Ostrenga, W. Teng, and S. Kempler (2012), Tropical Rainfall Measuring Mission (TRMM) precipitation data and services for research and applications, *Bull. Am. Meteorol. Soc.*, *93*(9), 1317–1325, doi:10.1175/BAMS-D-11-00152.1.

Liu, Y., J. Stanturf, and S. Goodrick (2010), Trends in global wildfire potential in a changing climate, *For. Ecol. Manag.*, *259*(4), 685–697, doi:10.1016/j.foreco.2009.09.002.

López-Saldaña, G., I. Bistinas, and J. M. C. Pereira (2014), Global analysis of radiative forcing from fire-induced shortwave albedo change, *Biogeosci. Discuss.*, *11*(5), 7775–7796, doi:10.5194/bgd-11-7775-2014.

Lyons, E. A., Y. Jin, and J. T. Randerson (2008), Changes in surface albedo after fire in boreal forest ecosystems of interior Alaska assessed using MODIS satellite observations, *J. Geophys. Res.*, *113*, G02012, doi:10.1029/2007JG000606.

Myhre, Y., J. Govaerts, M. Haywood, T. K. Berntsen, and A. Lattanzio (2005), Radiative effect of surface albedo change from biomass burning, *Geophys. Res. Lett.*, *32*, L20812, doi:10.1029/2005GL022897.

Myhre, G. D., et al. (2013), Anthropogenic and natural radiative forcing, in *Climate Change 2013: The Physical Science Basis. Contribution of Working Group I to the Fifth Assessment Report of the Intergovernmental Panel on Climate Change*, edited by T. F. Stocker et al., pp. 659–740, Cambridge Univ. Press, Cambridge, U. K., and New York.

Oris, F., H. Asselin, A. A. Ali, W. Finsinger, and Y. Bergeron (2013), Effect of increased fire activity on global warming in the boreal forest, *Environ. Rev.*, *22*(3), 1–14, doi:10.1139/er-2013-0062.

Pausas, J. G., and J. E. Keeley (2009), A burning story: The role of fire in the history of life, *Bioscience*, *59*(7), 593–601, doi:10.1525/bio.2009.59.7.10.

Pechony, O., and D. T. Shindell (2010), Driving forces of global wildfires over the past millennium and the forthcoming century, *Proc. Natl. Acad. Sci.*, *107*(45), 19167–19170, doi:10.1073/pnas.1003669107.

Pinty, B., M. M. Verstraete, N. Gobron, F. Roveda, and Y. Govaerts (2000), Do man-made fires affect Earth's surface reflectance at continental scales?, *Eos. Trans. AGU*, *81*(34), 381–389, doi:10.1029/00EO00281.

Randerson, J. T., et al. (2006), The impact of boreal forest fire on climate warming, *Science*, *314*(5802), 1130–1132, doi:10.1126/science.1132075.

Riaño, D., J. A. Moreno Ruiz, J. Barón Martínez, and S. L. Ustin (2007), Burned area forecasting using past burned area records and Southern Oscillation Index for tropical Africa (1981–1999), *Remote Sens. Environ.*, *107*(4), 571–581, doi:10.1016/j.rse.2006.10.008.

Ribeiro, N. S., H. H. Shugart, and R. Washington-Allen (2008), The effects of fire and elephants on species composition and structure of the Niassa Reserve, northern Mozambique, *For. Ecol. Manag.*, *255*(5–6), 1626–1636, doi:10.1016/j.foreco.2007.11.033.

Roberts, G., M. J. Wooster, and E. Lagoudakis (2009), Annual and diurnal african biomass burning temporal dynamics, *Biogeosciences*, *6*(5), 849–866, doi:10.5194/bg-6-849-2009.

Rodell, M., et al. (2004), The Global Land Data Assimilation System, *Bull. Am. Meteorol. Soc.*, *85*(3), 381–394, doi:10.1175/BAMS-85-3-381.

Romero-Ruiz, M., A. Etter, A. Sarmiento, and K. Tansey (2010), Spatial and temporal variability of fires in relation to ecosystems, land tenure and rainfall in savannas of northern South America, *Global Chang. Biol.*, *16*(7), 2013–2023, doi:10.1111/j.1365-2486.2009.02081.x.

Roy, D. P., L. Giglio, D. J. Kendall, and C. O. Justice (1999), Multi-temporal active-fire based burn scar detection algorithm, *Int. J. Remote Sens.*, *20*, 1031–1038.

Roy, D. P., Y. Jin, P. E. Lewis, and C. O. Justice (2005), Prototyping a global algorithm for systematic fire-affected area mapping using MODIS time series data, *Remote Sens. Environ.*, *97*(2), 137–162, doi:10.1016/j.rse.2005.04.007.

Roy, D. P., L. Boschetti, C. O. Justice, and J. Ju (2008), The collection 5 MODIS burned area product—Global evaluation by comparison with the MODIS active fire product, *Remote Sens. Environ.*, *112*(9), 3690–3707, doi:10.1016/j.rse.2008.05.013.

Rundel, P. W., M. T. K. Arroyo, R. M. Cowling, J. E. Keeley, B. B. Lamont, and P. Vargas (2016), Mediterranean biomes: Evolution of their vegetation, floras, and climate, *Annu. Rev. Ecol. Evol. Syst.*, *47*, 383–407, doi:10.1146/annurev-ecolsys-121415-032330.

Samain, O., L. Kergoat, P. Hiernaux, F. Guichard, E. Mougin, F. Timouk, and F. Lavenu (2008), Analysis of the in situ and MODIS albedo variability at multiple timescales in the Sahel, *J. Geophys. Res.*, *113*, D14119, doi:10.1029/2007JD009174.

Schaaf, C. B., et al. (2002), First operational BRDF, albedo nadir reflectance products from MODIS, *Remote Sens. Environ.*, *83*(1–2), 135–148, doi:10.1016/S0034-4257(02)00091-3.

Scholes, R. J., and S. R. Archer (1997), Tree-grass interactions in savannas, *Annu. Rev. Ecol. Syst.*, *28*(1), 517–544, doi:10.1146/annurev.ecolsys.28.1.517.

Scholes, R. J., D. E. Ward, and C. O. Justice (1996), Emissions of trace gases and aerosol particles due to vegetation burning in southern hemisphere Africa, *J. Geophys. Res.*, *101*(D19), 23,677–23,682, doi:10.1029/95JD02049.

Scholes, R. J., P. R. Dowty, K. Caylor, D. A. B. Parsons, P. G. H. Frost, and H. H. Shugart (2002), Trends in savanna structure and composition along an aridity gradient in the Kalahari, *J. Veg. Sci.*, *13*(3), 419–428.

Shongwe, M. E., G. J. van Oldenborgh, B. J. J. M. van den Hurk, B. de Boer, C. A. S. Coelho, and M. K. van Aalst (2009), Projected changes in mean and extreme precipitation in Africa under global warming. Part I: Southern Africa, *J. Clim.*, *22*(13), 3819–3837, doi:10.1175/2009JCLI2317.1.

Smit, G. N. (2004), An approach to tree thinning to structure southern African savannas for long-term restoration from bush encroachment, *J. Environ. Manage.*, *71*(2), 179–191, doi:10.1016/j.jenvman.2004.02.005.

Smith, A. M. S., M. J. Wooster, N. A. Drake, F. M. Dipotso, and G. L. W. Perry (2005), Fire in African savanna: Testing the impact of incomplete combustion on pyrogenic emissions estimates, *Ecol. Appl.*, *15*(3), 1074–1082, doi:10.1890/03-5256.

Tansey, K., et al. (2004), A global inventory of burned areas at 1 km resolution for the year 2000 derived from spot vegetation data, *Clim. Chang.*, *67*(2–3), 345–377, doi:10.1007/s10584-004-2800-3.

Tsuyuzaki, S., K. Kushida, and Y. Kodama (2009), Recovery of surface albedo and plant cover after wildfire in a *Picea mariana* forest in interior Alaska, *Clim. Chang.*, *93*(3–4), 517–525, doi:10.1007/s10584-008-9505-y.

van Altena, C., R. van Logtestijn, W. Cornwell, and H. Cornelissen (2012), Species composition and fire: Non-additive mixture effects on ground fuel flammability, *Front. Plant Sci.*, *3*, 63, doi:10.3389/fpls.2012.00063.

van der Werf, G. R., J. T. Randerson, G. J. Collatz, L. Giglio, P. S. Kasibhatla, A. F. Arellano, S. C. Olsen, and E. S. Kasischke (2004), Continental-scale partitioning of fire emissions during the 1997 to 2001 El Niño/La Niña period, *Science*, *303*(5654), 73–76, doi:10.1126/science.1090753.

van der Werf, G. R., J. T. Randerson, L. Giglio, G. J. Collatz, P. S. Kasibhatla, and A. F. Arellano Jr. (2006), Interannual variability in global biomass burning emissions from 1997 to 2004, *Atmos. Chem. Phys.*, *6*(11), 3423–3441, doi:10.5194/acp-6-3423-2006.

van der Werf, G. R., J. T. Randerson, L. Giglio, G. J. Collatz, M. Mu, P. S. Kasibhatla, D. C. Morton, R. S. DeFries, Y. Jin, and T. T. van Leeuwen (2010), Global fire emissions and the contribution of deforestation, savanna, forest, agricultural, and peat fires (1997–2009), *Atmos. Chem. Phys.*, *10*(23), 11707–11735, doi:10.5194/acp-10-11707-2010.

Viegas, D. X. (2002), Forest fire research & wildland fire safety: Proceedings of IV International Conference on Forest Fire Research/2002 Wildland Fire Safety Summit, Coimbra, Portugal, November 18–23, 2002, 2000 pp., IOS Press, Rotterdam, Netherlands.

Wylie, D., D. L. Jackson, W. P. Menzel, and J. J. Bates (2005), Trends in global cloud cover in two decades of HIRS observations, *J. Clim.*, *18*(15), 3021–3031, doi:10.1175/JCLI3461.1.

Xue, Y., R. W. A. Hutjes, R. J. Harding, M. Claussen, S. D. Prince, T. Lebel, E. F. Lambin, S. J. Allen, P. A. Dirmeyer, and T. Oki (2004), The Sahelian climate, in *Vegetation, Water, Humans and the Climate*, edited by P. Kabat et al., pp. 59–77, Springer, Berlin.